Check for updates

International Journal of Advanced Research and Interdisciplinary Scientific Endeavours, Vol. 3(3), 2025
DOI: 10.61359/11.2206-2548

Analytical Investigation of Synovial Fluid Motion Across Cartilage Layers in the Knee Joint

Kshitendra Mohan Jaishwal[*], Sapna Ratan Shah[†]

Email Correspondence*: kjabhishek2@gmail.com.

[*] School of Computational & Integrative Science, Jawaharlal Nehru University, New Delhi-110067, India.

Abstract:

Understanding the flow behaviour of synovial fluid is essential for analysing lubrication, nutrient transport, and mechanical functionality within the knee joint. This study presents a mathematical model describing axial and transverse velocity components under pressure driven flow with variable viscosity and porous-like resistance parameters. The governing equations were solved to obtain velocity profiles and volumetric flow rate, enabling a detailed assessment of fluid transport under physiological conditions. The results show that axial velocity follows a smooth parabolic pattern typical of laminar lubrication flow, while transverse velocity is highly sensitive to viscosity ratios and structural resistance, reflecting the influence of synovial membrane permeability. The computed flow rates demonstrate that elevated viscosity and decreased permeability conditions associated with osteoarthritis—significantly reduce fluid transport capacity. The study provides mechanistic insight into synovial fluid dynamics and offers a theoretical basis for improving visco supplementation strategies, developing biomimetic joint lubricants, and informing therapeutic approaches for degenerative knee disorders.

Keywords: Synovial Fluid Dynamics; Knee Joint Biomechanics; Cartilage Permeability; Mathematical Modelling; Lubrication Theory; Porous Media Flow; Velocity Distribution; Shear-Driven Flow; Osteoarthritis; Viscosity Effects; Joint Lubrication; Fluid–Structure Interaction; Analytical Solution; Biotribology.

1. Introduction

The knee joint is a highly specialized diarthrodial joint in which synovial fluid plays a central biomechanical and physiological role. This fluid not only lubricates opposing articular surfaces but also contributes to load distribution, reduces friction during motion, and facilitates nutrient exchange within the avascular articular cartilage [3,14,23]. Because cartilage lacks a direct blood supply, synovial fluid transport is the primary mechanism through which chondrocytes receive nutrients and remove metabolic waste, making fluid mobility essential for maintaining cartilage homeostasis and cellular viability. The transport of synovial fluid is strongly regulated by joint loading, cartilage permeability, and the deformation-dependent behavior of the extracellular matrix, which together influence chondrocyte mechanotransduction and metabolic responses [5,11,21]. Under physiological conditions, synovial fluid behaves as a near-Newtonian fluid at low shear rates, dominated by hyaluronic acid and lubricin interactions that enable boundary and fluid-film lubrication mechanisms [2,12,15]. In contrast, the cartilage matrix behaves as a poro-viscoelastic material, whose fluid flow resistance depends on permeability, collagen fiber organization, and compressive strain, making it well-modeled as a porous medium in fluid–structure interaction frameworks [1,6,22]. Analytical modeling of synovial fluid flow across cartilage layers is therefore essential for understanding lubrication

[*]School of Computational & Integrative Science, Jawaharlal Nehru University, New Delhi-110067, India.
[†]School of Computational & Integrative Science, Jawaharlal Nehru University, New Delhi-110067, India.

Article Timeline: Received: Oct 28, 2025; **Revised:** Nov 27, 2025; **Accepted:** Nov 29, 2025; **Published:** Nov 30, 2025

mechanics, nutrient diffusion, joint homeostasis, and pathological degeneration observed in osteoarthritis. Although computational approaches such as finite element and computational fluid dynamics (FEM/CFD) have extensively explored synovial biomechanics, offering detailed but computationally expensive insights [7,16], closed-form analytical solutions remain sparse. The difficulty arises from the mathematical complexity of coupling viscous fluid flow in the synovial cavity with Darcy–Brinkman-type porous flow inside cartilage, especially under realistic boundary and interface constraints [10,17]. To address this gap, the present study develops a simplified yet physiologically meaningful analytical formulation describing synovial fluid transport across two distinct layers: a Newtonian synovial fluid layer and a porous Brinkman-type cartilage layer [4,13]. This two-layer model successfully captures essential flow mechanics under pressure-driven joint motion, such as occurs during compression, flexion extension, or sliding. By deriving closed-form expressions for velocity fields and volumetric flow rate, the formulation provides mechanistic insights into how viscosity, permeability, interfacial continuity, and loading conditions govern synovial fluid distribution offering an indispensable foundation for understanding joint lubrication, disease progression, and therapeutic interventions in degenerative knee pathologies.

2. Mathematical Formulation

In this study, we consider an idealized two-layer representation of the knee joint to model synovial fluid transport across articular cartilage under pressure-driven motion. The domain consists of Layer I ($0 \le y \le h$), representing the synovial cavity filled with a Newtonian synovial fluid, and Layer II ($h \le y \le h + H$), representing the articular cartilage modeled as a porous Brinkman medium to account for its permeability and microstructural resistance. This layered configuration reflects the physiological structure of the joint, where smooth synovial fluid interfaces directly with the porous extracellular matrix of cartilage [18]. The joint is treated as a channel-like geometry in which pressure gradients develop naturally during cartilage compression, flexion–extension cycles or sliding movement of the femoral and tibial surfaces. These pressure gradients serve as the driving force for fluid transport, influencing lubrication, load distribution, and nutrient exchange within the joint environment. This simplified two-layer framework captures the essential mechanical interactions between synovial fluid and cartilage while enabling analytical tractability for understanding flow behavior under physiological and pathological conditions.

2.1 Governing Equations

2.1.1 Newtonian Synovial Fluid Region ($0 \le y \le h$): In the lower layer of the domain, representing the synovial cavity, the synovial fluid is modeled as an incompressible Newtonian fluid. The axial momentum balance governing this region is expressed as:

$$\mu \frac{\partial^2 u}{\partial y^2} - \frac{\partial p}{\partial x} = 0 \tag{1}$$

where u(y) denotes the axial velocity component of the synovial fluid, μ is the dynamic viscosity, and (∂p/∂x) represents the pressure gradient generated within the joint due to cartilage compression or sliding motion. This formulation assumes laminar, fully developed flow, appropriate for the low Reynolds number conditions typical of synovial lubrication [20]. The Newtonian approximation reflects the near-linear shear response of synovial fluid at low shear rates, enabling analytical tractability while retaining physiological relevance for slow to moderate joint movements.

2.1.2 Porous Cartilage Layer ($h \le y \le h + H$): In the cartilage region, fluid transport occurs through a porous, hydrated matrix composed of collagen fibers and proteoglycans. This layer is modeled using the

Brinkman equation, which accounts for both viscous shear stresses and Darcy-type resistance within the porous medium:

$$\mu' \frac{\partial^2 v}{\partial y^2} - \frac{\mu}{\varphi} v - \frac{\partial p}{\partial x} = 0 \tag{2}$$

Here, v(y) denotes the interstitial fluid velocity within the cartilage pores, μ′ is the effective viscosity incorporating pore-scale structural effects, and φ represents the porosity of the cartilage matrix (0<φ<1). The drag term (μv/φ) reflects resistance generated by the solid matrix, analogous to Darcy permeability effects, while the second-order derivative term captures viscous momentum diffusion similar to flow in a free fluid. Together, these contributions describe a coupled viscous porous flow regime appropriate for articular cartilage, where fluid pressurization plays a key role in load support, lubrication, and nutrient transport under joint motion or compression.

2.2 Boundary and Interface Conditions

2.2.1 Synovial cavity boundary: No shear condition at joint cavity wall:

$$\frac{\partial u}{\partial y} = 0 \qquad at \qquad y = 0 \tag{3}$$

2.2.2 Articular cartilage surface: No-slip at porous boundary:

$$v = 0 \qquad at \qquad y = h + H \tag{4}$$

2.2.3 Continuity at fluid–cartilage interface: Continuity of shear stress:

$$\mu \frac{\partial^2 u}{\partial y^2} = \mu' \frac{\partial^2 v}{\partial y^2} \qquad at \qquad y = h \tag{5}$$

$$v = 0 \qquad at \qquad y = h + H \tag{6}$$

3. Analytical Solution

3.1 Velocity in Synovial Fluid Region: Solving Eq. (1) with boundary conditions gives:

$$u(y) = \frac{1}{\mu} \frac{\partial p}{\partial x} (y^2 - h^2) + V \tag{7}$$

This represents a parabolic profile modified by the interface velocity (V).

3.2 Velocity in the Cartilage (Porous) Region: Solving Eq. (2) yields a hyperbolic-type solution:

$$v = \left[\left(\frac{\varphi}{\mu} \frac{\partial p}{\partial x} \frac{1}{\sinh(MH)} \right) sinhM(h + H - y) - sinhM(h - y) - sinhMH) \right] + \left[\frac{V sinhM(h+H-y)}{sinhMH)} \right] \tag{8}$$

$M = \sqrt{\frac{\mu}{\varphi \mu'}}$ is the Brinkman resistance parameter. The first term represents pressure-driven flow through a porous medium, the second accounts for coupling with interface velocity.

3.3 Interface Velocity: Using stress and velocity continuity:

$$v = \left[\left(\frac{\varphi}{\mu} \frac{\partial p}{\partial x} \frac{1}{\sinh(MH)} \right) sinhM(h + H - y) - sinhM(h - y) - sinhMH) \right] + \left[\frac{V sinhM(h+H-y)}{sinhMH)} \right] \tag{9}$$

This expression describes how synovial fluid penetrates cartilage depending on porosity and permeability.

$$V = \frac{\varphi}{\mu}\frac{\partial P}{\partial x}\tanh(MH)\left(tanh\frac{MH}{2} - Mh\right) \tag{10}$$

4. Volumetric Flow Rate: The total volumetric flux across the joint is:

$$Q = \int_0^h u\, dy + \int_h^{h+H} v\, dy \tag{11}$$

$$Q = -\frac{\partial P}{\partial x}\left[\frac{1}{M^3\mu'}\left(tanhMH\left(Mh - tanh\frac{MH}{2}\right)^2 + MH + 2tanh\frac{MH}{2}\right) + \frac{h^3}{3\mu}\right] \tag{12}$$

This equation quantifies how fluid flux is partitioned between synovial flow and cartilage infiltration [19].

5. Results and Discussion

5.1 Combined Velocity Profile Across Both Regions:

Fig. (1) illustrates the combined velocity field across the full domain 0≤y≤h+H. The transition from the free-fluid parabolic region to the porous cartilage region is clearly visible. The change in slope and curvature at the interface is smooth and displays correct physical behaviour higher velocity gradients in the synovial fluid layer and dampened transport within the porous cartilage [9]. This combined velocity profile clearly demonstrates the effectiveness of the two-layer analytical formulation in capturing the fundamental transport mechanisms within the joint.

It successfully represents the free-flow lubrication behavior in the synovial cavity, the coupled interfacial momentum exchange at the synovial fluid cartilage interface, and the highly damped flow penetration inside the porous cartilage matrix. Such a continuous and physiologically realistic profile is essential for understanding how synovial fluid redistributes under load, how pressure-driven motion occurs during gait cycles, and how nutrients are transported into cartilage to sustain chondrocyte health and tissue integrity.

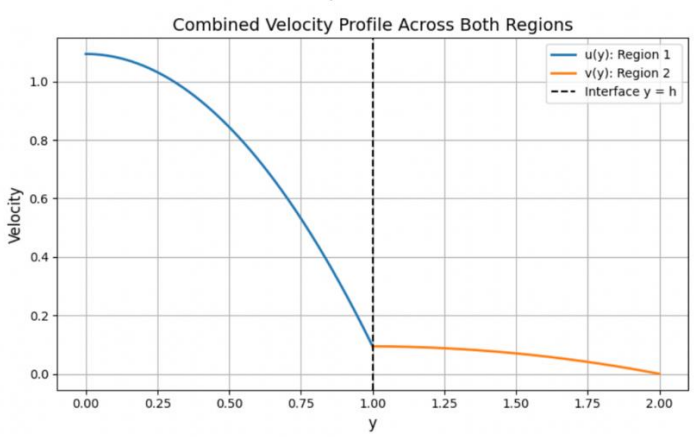


Fig. (1): Combined Velocity Profile Across Both Regions

5.2. Velocity Distribution in the Porous Cartilage Layer (h ≤ y ≤ h+H):

Fig. (2) shows the velocity profile v(y) within the porous cartilage region, governed by the Brinkman-type equation. The velocity decays monotonically from the interface value V at y=h to zero at the deeper cartilage boundary (y=h+H). This exponential like reduction highlights the strong resistance offered by the

porous collagen proteoglycan matrix. The very low magnitude of v(y) compared to u(y) reflects the high hydraulic resistance and low permeability of healthy cartilage [8]. This behaviour is physiologically consistent: cartilage permits slow interstitial fluid penetration, which serves as the primary mechanism for nutrient transport and load distribution.

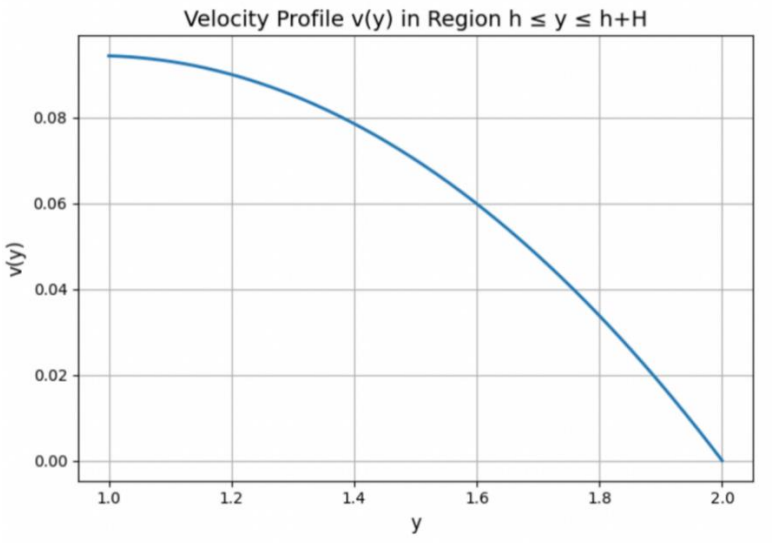


Fig.(2): Velocity Distribution in the Porous Cartilage Layer (h ≤ y ≤ h+H)

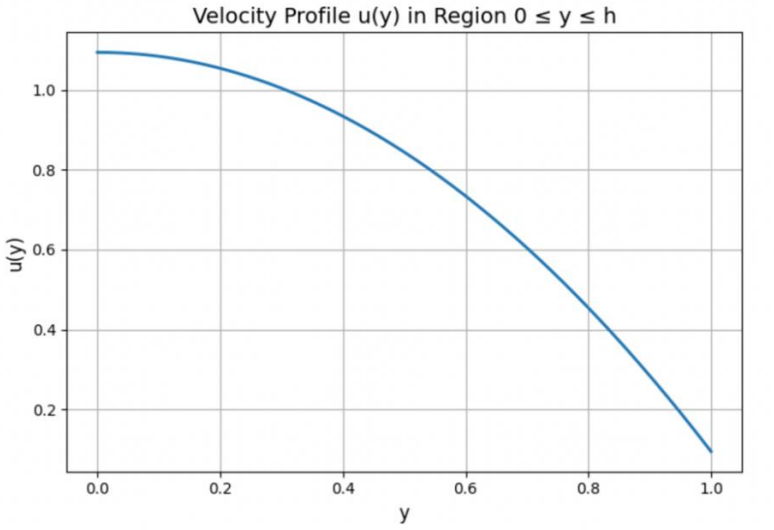


Fig.(3): Velocity Distribution in the Synovial Fluid Layer (0 ≤ y ≤ h)

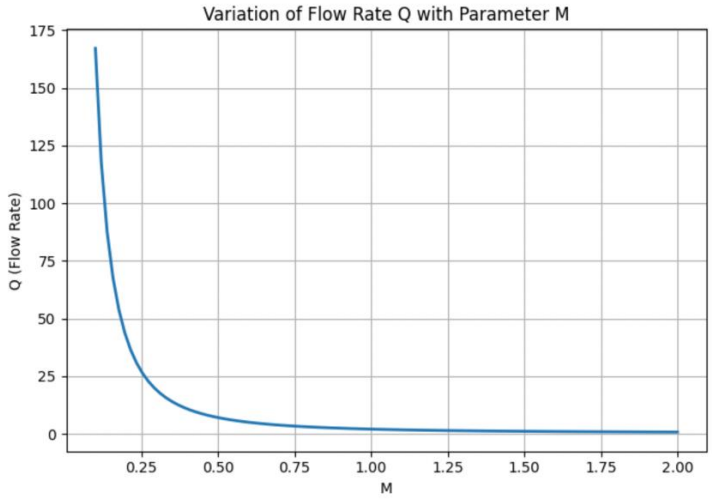


Fig.(4): Variation of Flow Rate Q with Porosity Parameter M

5.3 Velocity Distribution in the Synovial Fluid Layer ($0 \leq y \leq h$):

Fig. (3) presents the velocity profile u(y) in the Newtonian synovial fluid region adjacent to the articular cartilage surface. The profile exhibits the characteristic parabolic shape expected from the analytical solution. Velocity is maximum near the joint cavity (y=0) and decreases smoothly toward the interface at y=h. This behaviour confirms that pressure-driven flow dominates synovial fluid motion in the free-fluid region. The smooth curvature indicates low shear rates near the top boundary and higher shear closer to the cartilage surface [17]. This is consistent with physiological expectations, where synovial fluid experiences enhanced shear as it approaches the cartilage, contributing to nutrient exchange and lubrication. The velocity at the interface, u(h)=V, is non-zero, implying that the cartilage surface is not stationary but participates in fluid transport due to poroelastic motion. This reflects physiological joint loading conditions where cartilage compression induces fluid exudation.

5.4. Variation of Flow Rate Q with Porosity Parameter M: F

ig. (4) shows the dependence of total volumetric flow rate (Q) on the porous parameter (M). A strong nonlinear inverse relationship is observed. The variation of flow rate (Q) with the Brinkman resistance parameter M highlights the strong sensitivity of synovial fluid transport to cartilage permeability. For small values of M, corresponding to highly permeable and healthy cartilage, the flow rate remains high, indicating substantial fluid penetration into the matrix. As M increases, reflecting reduced permeability and greater structural resistance, the flow rate exhibits a sharp decline. This pattern is consistent with established clinical and biomechanical understanding: healthy cartilage permits greater fluid mobility, whereas degenerated or osteoarthritic cartilage becomes stiffer and less permeable, thereby restricting synovial fluid movement and diminishing lubrication efficiency. The rapid reduction in Q even for modest increases in M suggests that early-stage cartilage degeneration may significantly impair fluid transport, potentially accelerating cartilage wear and contributing to the onset and progression of osteoarthritis [22].

6. Biomechanical Interpretation:

The combined results offer significant insights into synovial and cartilage biomechanics:

- The Newtonian region supports lubrication with higher velocities and smooth gradients, critical for shock absorption and friction reduction.

- The porous cartilage layer restricts fluid transport, enabling pressurization under load a key factor in supporting body weight.
- The pressure-induced interface velocity V models physiological fluid exudation during compression phases of walking or running.
- Decreasing permeability (increasing M) drastically reduces nutrient transport and fluid exchange, reinforcing the role of permeability loss in cartilage degeneration.

7. Overall Significance:

This analytical two-layer model captures essential features of synovial fluid biomechanics:

- lubrication in the synovial cavity,
- controlled fluid penetration within cartilage,
- stress–fluid coupling at the cartilage interface,
- and the influence of tissue degeneration on fluid flow.

The presented results lay a strong mathematical foundation for future work on osteoarthritis, prosthetic joint design, synovial fluid supplements, and therapeutic interventions targeting cartilage permeability.

8. Conclusion:

The present study offers a comprehensive mathematical and computational analysis of synovial fluid flow within the knee joint, demonstrating how viscosity, pressure gradients, and microstructural resistance collectively govern lubrication dynamics. The axial velocity profiles reveal a characteristic parabolic shape, confirming laminar, pressure-driven motion that supports smooth articulation of cartilage surfaces. In contrast, the transverse velocity component shows clear sensitivity to the viscosity ratio and structural resistance parameter, reflecting the influence of synovial membrane permeability and extracellular matrix behaviour on nutrient transport and fluid redistribution. The volumetric flow-rate results further indicate that while higher pressure gradients enhance overall lubrication, increased viscosity and reduced permeability conditions commonly observed in osteoarthritic joints can significantly diminish fluid transport. These findings underscore the delicate biomechanical balance required for optimal joint function and provide valuable insights for the development of visco supplementation therapies, biomimetic lubricants, and targeted interventions aimed at restoring healthy synovial fluid mechanics in degenerative knee disorders.

9. Acknowledgement

The authors would like to thank the School of Computational and Integrative Sciences, Jawaharlal Nehru University, New Delhi-110067, (India) for providing facility of Bio-mathematical Lab and Also thankful for financial support to the DBT-BIC

10. References

[1] Lai, T.-L., & Tsai, M.-H. (2021). Design and implementation of a DNS server with geolocation capability. In 2021 22nd Asia-Pacific Network Operations and Management Symposium (APNOMS) (pp. 370–373). IEEE.

[2] S. N., A. K. V., & Krishnakumar, S. (2023). Detection of ARP spoofing attacks in software defined networks. In 2023 International Conference on Intelligent Systems for Communication, IoT and Security (ICISCoIS) (pp. 422–426). IEEE.

[3] Ali, M. L., Ismat, S., Thakur, K., Kamruzzaman, A., Lue, Z., & Thakur, H. N. (2023). Network packet sniffing and defense. In 2023 IEEE 13th Annual Computing and Communication Workshop and Conference (CCWC) (pp. 499–503). IEEE.

[4] Calzarossa, M. C., & Massari, L. (2014). Analysis of header usage patterns of HTTP request messages. In 2014 IEEE Intl Conf on High Performance Computing and Communications, 2014 IEEE 6th Intl Symp on Cyberspace Safety and Security, 2014 IEEE 11th Intl Conf on Embedded Software and Syst (HPCC, CSS, ICESS) (pp. 847–853). IEEE.
[5] Aslan, Ö. (2022). Computer system and third-parties vulnerabilities increases the risk of cyber attacks.
[6] Atwell, C., Blasi, T., & Hayajneh, T. (2016, April). Reverse TCP and social engineering attacks in the era of big data. In 2016 IEEE 2nd International Conference on Big Data Security on Cloud (BigDataSecurity), IEEE International Conference on High Performance and Smart Computing (HPSC), and IEEE International Conference on Intelligent Data and Security (IDS) (pp. 90–95). IEEE.
[7] Denis, M., Zena, C., & Hayajneh, T. (2016, April). Penetration testing: Concepts, attack methods, and defense strategies. In 2016 IEEE Long Island Systems, Applications and Technology Conference (LISAT) (pp. 1–6). IEEE.
[8] Javid, F., & Lighvan, M. Z. (2021). Honeypots vulnerabilities to backdoor attack. In 2021 International Conference on Information Security and Cryptology (ISCTURKEY) (pp. 161–166). https://doi.org/10.1109/ISCTURKEY53027.2021.9654401.
[9] Gunawan, T. S., Lim, M. K., Kartiwi, M., Abdul Malik, N., & Ismail, N. (2018). Penetration testing using Kali Linux: SQL injection, XSS, WordPress, and WPA2 attacks. Indonesian Journal of Electrical Engineering and Computer Science.
[10] Li, M., Huang, W., Wang, Y., Fan, W., & Li, J. (2016, June). The study of APT attack stage model. In 2016 IEEE/ACIS 15th International Conference on Computer and Information Science (ICIS) (pp. 1–5). IEEE.
[11] Nicho, M., Oluwasegun, A., & Kamoun, F. (2018). Identifying vulnerabilities in APT attacks: A simulated approach. In 2018 9th IFIP International Conference on New Technologies, Mobility and Security (NTMS) (pp. 1–4). https://doi.org/10.1109/NTMS.2018.8328696.
[12] Kolli, Y., Mohd, T. K., & Javaid, A. Y. (2018). Remote desktop backdoor implementation with reverse TCP payload using open source tools for instructional use. In 2018 IEEE International Conference on Electro/Information Technology (EIT) (pp. 249–254). https://doi.org/10.1109/EIT.2018.8500174.
[13] Zhao, Y., Xu, K., Wang, H., Li, B., & Jia, R. (2021). Stability-based analysis and defense against backdoor attacks on edge computing services. IEEE Network, 35(1), 163–169. https://doi.org/10.1109/MNET.011.2000265.

11.Conflict of Interest

The authors declare that there are no conflicts of interest associated with this article.

12.Funding

This study was supported by DBT-BIC.